Supplemental Information

Edwards et al.

1 Experimental Methods

1.1 Myocyte isolation:

Myocytes were isolated from the LV and septum essentially as previously[17]. Collagenase concentration was 2 mg/mL (type 2, Worthington), and BDM was excluded throughout. Briefly, animals were heparinized (10 IU ip) 10-15 minutes before the heart was excised under isoflurane anaesthesia (3%). The heart was retrograde perfused under constant flow ($\sim$3 mL/min), with nominally Ca^{2+} free solution (mmol/L: 113 NaCl, 4.7 KCl, 0.6 KH_2PO_4, 0.6 Na_2HPO_4, 1.2 $MgSO_4$, 12 $NaHCO_3$, 10 $KHCO_3$, 10 hepes, 5.5 D-glucose, and Taurine 30). After 5 minutes, the perfusate was switched to enzyme and Ca^{2+} (12.5 μmol/L) containing solution for a further 15 minutes. The heart was then cut down, teased apart, and triturated in collagenase-free solution supplemented with calf serum (FCS, 5%). Cells were plated in minimum essential media (0.5% FCS) on laminin coated (1 $\mu g/cm^2$) glass coverslips. Once seeded, cells were stored at 37° C in serum-free media (0.5 mM Ca^{2+}, pH 7.4) for use within the following 2 - 8 hours.

1.2 Experimental solutions:

As described in the Methods, the external solution (Normal Tyrode's, NT) for all myocyte experiments contained (mmol/L) 140 NaCl, 4 KCl, 1 $CaCl_2$, 1 $MgCl_2$, 10 D-glucose, and 10 Hepes (pH: 7.4, NaOH). Isoproterenol (100 nmol/L) was added from frozen stock (1 mmol/L in 0.01N HCl), and caffeine (10 mmol/L) was prepared fresh from powder. The internal solution contained (mmol/L) 140 K-Aspartate, 10 KCl, 10 NaCl, 5 Mg-ATP, 1 $MgCl_2$, 0.3 Li-GTP, and 125 μmol/L Fura-2 potassium salt (pH 7.2, KOH).

1.3 Patch-clamping:

Whole-cell current-clamping was performed on visually quiescent, rod-shaped myocytes, with clear striations. High-resistance patch microelectrodes (8-13 MOhm with this internal solution) were pulled from borosilicate glass and used in fast I-clamp mode of an Axopatch 200B amplifier, controlled by pClamp 6 software and a Digidata 1200A interface. Membrane potential (E_m) was sampled at 5 kHz and Bessel filtered at 1 kHz. Measured ($\sim$ 10 mV) liquid junction potential was used for *a priori* correction of E_m.

Fast capacitance was corrected in the cell-attached configuration. After gaining access, series resistance (R_s), which averaged 18.9 MOhms and was not different between Tg (19.2 $\pm$ 1.0) and WT (18.2 $\pm$ 1.2), was corrected for pacing current injection (1-2 ms, 0.5-2 nA square-wave pulses). Cells were then paced for 50 cycles (1 Hz) in NT before Iso was applied focally by 250 micron diameter micro-bore tubing. Another 50 cycles were acquired at least 1 minute after beginning Iso superfusion. The bathing solution was maintained at 37° C throughout, and the experimenter was blinded to the genotype of the cells.

1.4 Ca^{2+} epifluorescence:

Fura-2: As noted above, the internal solution contained free Fura-2 to limit dye diffusion into the pipette. An Ion Optix fluorescence system equipped with optics appropriate for Fura-2 (340/380 nm excitation, 510 nm emission) was interfaced with the patch-clamp acquisition system to synchronize the E_m and fluorescence signals. Initial F340/F380 was calculated after background subtraction at each excitation wavelength, and then 1st order Savitzky-Golay filtered to give the final ratio time-series.

Fluo-3: Fluo-3 fluorescence was excited at 480 nm and 535 nm emission was collected at 1 kHz. All recordings were background subtracted and normalized to mean diastolic Ca^{2+}concentration (F_0) during the 1 Hz pacing period.

1.5 Echocardiography:

Short-axis M-mode echocardiograms were recorded with an Agilent Technologies Sonos 5050 system and S12 pediatric probe (12 MHz, Philips). Animals were isoflurane anesthetized (1 - 1.5% maintenance) and warmed by a circulated water pad. M-mode data were collected at a depth of 2 cm, a sweep speed of 150 mm/s, and averaged over at least 3 full cycles. All data collection and analyses were performed by the same trained technician.

1.6 ECG:

Mice were tribromoethanol (2.5%) anesthetized, warmed, and instrumented for 3-lead ECG (limb needle electrodes) and Isoproterenol (Iso) challenge by tail vein infusion. The pseudo-lead 1 signal was externally conditioned by a Humbug noise cancellation unit (Quest Scientific, Vancouver), and recorded at 10 kHz. After 2 minutes of baseline recording, Iso (25 μg/kg) was administered in warmed physiologic saline by low volume ($\sim$ 0.05 cc) bolus infusion over 20 seconds, and the recording was continued for a further 8 minutes. Steady state ECG parameters were measured from 10-second epochs occurring at the beginning of minutes 1, 3, 5, 7, and 9, by custom Matlab software. For each epoch, all cycles (n $\sim$ 60 to 100) were temporally aligned by the peak of the R-wave and averaged to give a smooth mean ECG waveform. Features of interest were manually identified by the same blinded analyst. The rate-corrected QT interval was calculated as by Mitchell *et al*. 1998[16]: QT_c = Q-T_0/(R-R_0/100)$^{1/2}$. PVCs and other arrhythmia were visually identified by

a blinded analyst over the entire time-course. Ventricular tachycardia (VT) was defined as > 4 PVCs in sequence, and separated into non-sustained (< 30 s), and sustained episodes ($>= 30$ s). Because very few ectopic events were observed under Iso challenge alone, a separate cohort received intraperitoneal injection of both caffeine (120 mg/kg) and epinephrine (2 mg/kg).

1.7 Analyses:

Early (EADs) and delayed afterdepolarizations (DADs) were identified by the same blinded analyst. Recordings for which EADs occurred in more than 10% of cycles were defined as EAD+, no recording exhibited DADs in more than 5% of cycles. In addition to conventional EAD and DAD morphologies, we observed a number of sustained events (SEs) that lasted 3 or more pacing cycles - Figure S9. Like DADs, these were infrequent (24 events in total), but unlike DADs they were more frequent in Tg cells during Iso challenge. Roughly equal numbers of SEs initiated spontaneously (11/24) as were triggered via the patch electrode (13/24). Because triggered SEs were indistinguishable from conventional EADs other than that they failed to terminate within one full cycle, we considered them a special class of EAD for all analyses. For each cell, steady state action potential and Ca^{2+} transient characteristics were averaged over the final 5-10 stable cycles for each of the Iso and baseline recordings. In EAD+ recordings this period directly preceded initiation of EADs. For pause-induced SCR experiments, SCR events were manually identified by the same blinded analyst. SCR events less than 10% of the pacing Ca^{2+} transient amplitude were thresholded out of all further analyses.

2 Computational mouse model:

The objective of our mouse myocyte model was to identify the current carrier/s likely to be responsible for EAD initiation. The base electrophysiologic model was the Bondarenko mouse myocyte[5], including recent updates[4]. We modified this model either to improve general functional characteristics, or permit more straightforward fitting to our data. First we replaced several key Ca^{2+} handling mechanisms and reparameterized a number of other sarcolemmal current carriers to better reflect established characteristics of murine Ca^{2+} handling, improve model stability, or emulate our experimental conditions (e.g. physiologic temperature). Second, we parameterized this new Baseline model to yield a transgenic (Tg) model fit to data presented here or published previously. Lastly, we imposed a further parameter set to represent established effects of acute β-adrenergic challenge. The final parameter changes applied to each of these three stages of development are provided in Table 1.

2.1 Baseline modifications

The Bondarenko model provides a detailed foundation for this study, and was recently extended by Li *et al*.[11]. We adopt several of their alterations, but have also diverged in a number of places to better fit data specifically collected at 1 Hz in CaMKIIδ_C-transgenic cells.

Our major changes were made to correct Ca^{2+}-handling mechanisms and achieve appropriate Ca^{2+} flux balance. We have replaced the original formulations of I_{NaCa}, SERCA, RyR, and I_{Na}. Our I_{NaCa} implementation is a modified version of the Weber *et al*. model (W-B)[21]. The models of SR Ca^{2+} release and reuptake are slight deviations from those of the Shannon-Bers myocyte (S-B)[19], and the I_{Na} model is identical to that developed by Grandi *et al*.[7] (G-B), and was chosen to incorporate CaMKII-specific regulatory effects at this current.

As in the L-S model, we also reparameterized the plasma membrane Ca^{2+}-ATPase (PMCA) and Na^+/K^+-ATPase, to reduce overall Ca^{2+} extrusion to between 0.5 and 1%, and prevent progressive Na^+ overload, respectively. These and other simple parameter changes are presented in supplemental table 1.

2.1.1 Na^+/Ca^+ exchange

Our goal in reimplementing I_{NaCa} was to simultaneously match our experimental $[Ca^{2+}]_i$ decay kinetics, maintain realistic murine flux distribution between NCX and SERCA, and permit $[Ca^{2+}]_i$-dependent regulation of APD_{90}. We have taken an approach similar to Livshitz *et al*.[12], who distributed a fraction (β) of the recruitable I_{NaCa} to the same functional compartment as I_{Ca_L} and SR Ca^{2+} release. Those authors used this definition to account for the well-known effects of intracellular Ca^{2+} gradients upon I_{NaCa} and I_{Ca_L} inactivation kinetics. We chose it both to provide some functionalistic account for these gradients during the AP, and to retain simple parameterization of I_{NaCa} (2 free parameters). Finally, as in Li *et al*.,[11] and because $[Ca^{2+}]_i$-dependent regulation was not originally observed in intact mouse myocytes, we did not include the allosteric term of the original W-B model[21]. We note that this form of regulation has been observed in murine excised patches[15], and that this discrepancy remains unresolved, but may be explained by a higher affinity of the cytosolic regulatory site in the mouse, which would leave allosteric regulation near-saturated at diastolic $[Ca^{2+}]_i$[21]. Our final formulation was:

$$I_{NaCa} = V_{NCX}\left(\beta\Delta E_{ss} + (1-\beta)\Delta E_i\right) \tag{1}$$

where β is the fraction of NCX sensing dyadic subspace $[Ca^{2+}]([Ca^{2+}]_{ss})$, and both ΔE_{ss} and ΔE_i represent the electrochemical contributions to I_{NaCa} resulting from the subspace and bulk myoplasmic

concentrations, respectively. These are calculated as by Weber *et al.*[21], where x refers to either ss or i:

$$\Delta E_x = \frac{([Na]_i^3[Ca]_o e^{\frac{\eta VF}{RT}} - [Na]_o^3[Ca]_x e^{\frac{(\eta-1)VF}{RT}})}{\left(\begin{array}{c} K_{mCa_o}[Na]_i^3 + K_{mNa_o}^3[Ca]_x + K_{mNa_i}^3[Ca]_o(1 + \frac{[Ca]_x}{K_{mCa_i}}) \\ +K_{mCa_i}[Na]_o^3(1 + \frac{[Na]_i^3}{K_{mNa_i}^3}) + [Na]_i^3[Ca]_o + [Na]_o^3[Ca]_x \end{array} \right) \left(1 + k_{sat} e^{\frac{(\eta-1)VF}{RT}}\right)} \quad (2)$$

V_{NCX} and β were the only free parameters for parameterization, which is described further in section 2.2.

2.1.2 RyR

Two key features of Tg-specific Ca^{2+}-handling are enhanced fractional release and markedly reduced SR Ca^{2+} load[9,14,22]. To represent these characteristics we replaced the Bondarenko RyR gating scheme with the S-B four-state model[19], which incorporates a more readily modifiable sensitivity to SR luminal Ca^{2+}. The structure of the receptor was unchanged from the original S-B version, but it was parameterized to operate within the relatively low peak $[Ca^{2+}]_{ss}$ of the Bondarenko model - supplemental table 1. To more easily retain graded release and prevent prolonged SR Ca^{2+} release events, both of which involve ensemble effects that can only be approximated by a common pool SR release structure, we inherited the gaussian expression for P_{RyR} from Bondarenko *et al.*,[4]. One outcome of this choice is that we may have limited our ability to replicate the sustained EC coupling involved in the plateau period of type 1 EADs observed in our experiments. Less constrained SR Ca^{2+} release formulations may be required to achieve this type of behavior. Otherwise our final formulation for SR Ca^{2+} release flux remains standard:

$$J_{rel} = k_s P_o([Ca]_{jsr} - [Ca]_{ss})P_{RyR} \quad (3)$$

$$\frac{dP_{RyR}}{dt} = -0.02P_{RyR} - 0.1(\frac{I_{Ca_L}}{I_{Ca_{L,max}}})e^{(\frac{-V}{30})} \quad (4)$$

2.1.3 SERCA

Our motivation for replacing Bondarenko's forward-only Hill-type expression for SERCA with the S-B model was to impose thermodynamic constraint on maximal SR Ca^{2+} load. This was because our experiments suggest that increased SR Ca^{2+} release, SR Ca^{2+} reuptake rate, and therefore SR Ca^{2+} load, are key determinants of EAD initiation during β-adrenergic challenge. In the case of forward-only Hill-type formulations, SERCA-mediated Ca^{2+} re-uptake is balanced by dissipative flux (non-SERCA-mediated SR leak flux) at equilibrium (maximum) SR load. Alternatively, the S-B model imposes a limit to SR load defined by $\Delta G_{ATP} \times \epsilon_{SERCA}$, where ΔG_{ATP} is the free energy of ATP hydrolysis, and ϵ_{SERCA} is the efficiency of forward SERCA transport. This approach provides an intrinsic means of constraining maximal SR Ca^{2+} load.

2.1.4 I_{Na}

As described above, we exchanged the Bondarenko I_{Na} model for the G-B model[7], and specifically fit to Tg mice in Wagner *et al.*,[20]. The scheme and paramaterization used here is identical to that of Wagner *et al.*,[20].

2.2 Fitting:

2.2.1 Calcium Handling

In addition to the data presented here, we used 2 prior studies to fit SR Ca^{2+} load and EC coupling characteristics of Baseline and Tg models (without Iso). Maier *et al.*[14] provides data from the CaMKIIδ_C-Tg mice late in HF progression, thus including both acute CaMKII effects and pronounced HF remodeling. Kohlhaas *et al.*[9], examined the acute effects of CaMKIIδ_C overexpression on Ca^{2+}-handling mechanisms in rabbit myocytes. We considered the effects that were consistent between these 2 studies, and our current data, to be attributable only to acute CaMKII hyperactivity. These can be summarized as:

1. Reduced SR Ca^{2+} load, and increased diastolic SR Ca^{2+} leak
2. Increased fractional release (FR)
3. Slowed I_{CaL} inactivation, and slightly increased peak I_{CaL}

The differences in SR Ca^{2+} handling between Baseline and Tg models were fit to the current data set. While we did not directly measure I_{Ca_L} in this study, the differences resulting from CaMKIIδ_C overexpression for both prior studies were quantitatively similar, and suggest that the major macroscopic effects of CaMKII at I_{Ca_L} occur independent of HF remodeling. As such, we fitted the Baseline and Tg models to exhibit differences in I_{Ca_L} dynamics that were intermediate to the differences observed in those two studies. We did not reduce the Baseline peak I_{Ca_L} conductance from the Bondarenko model, which was higher than that observed by either Kohlhaas *et al.* or Maier *et al.*., because this would also have required much broader (and poorly constrained) reparameterization of the K^+ current conductances.

Figure S1 shows the final characteristics of steady-state Ca^{2+} handling in the Baseline and Tg models as well as those of Kohlhaas *et al.*[9] and Maier *et al.*[14]. Supplemental table 1 gives the model parameters used to achieve this behavior. Briefly, matching 90:10 % (SERCA:NCX) flux balance and experimental τ_{Ca} was achieved in the Baseline model by decreasing V_{NCX} by $\approx$ 50%, setting β = 0.3, and reducing V_{SERCA} to 200 μmol/L cytosol/ms. Additionally, setting K_{mf} = 0.6 $\mu mol/L$ and K_{mr} = 3500 $\mu mol/L$, gave Baseline diastolic $[Ca]_i \approx$ 120 nmol/L, and an equilibrium ratio, $[Ca]_{SR} : [Ca]_i$, of 5833. This implies 75% SERCA efficiency, which is similar to experimental observations and the original parameterization of this model[19]. The free parameters used to simultaneously reduce SR Ca^{2+} load and increase fractional release in the Tg model were: 1) EC_{50SR} (RyR sensitivity to luminal Ca^{2+}), 2) k_{leak} (SR Ca^{2+} leak permeability), 3) V_{NCX}, and 4) V_{SERCA}. EC_{50SR} and k_{leak} represent demonstrated CaMKII effects at RyR[1,6,22], V_{NCX} and V_{SERCA}

represent remodeling effects that are associated with chronic CaMKII overexpression[14] and are possibly directly dependent upon CaMKII-mediated transcriptional regulation[13]. Figure S2 shows that these changes shifted Ca^{2+} flux balance to favor NCX-mediated extrusion, although SERCA-mediated Ca^{2+} reuptake still accounted for $\sim$ 80% of cytosolic Ca^{2+} removal.

2.2.2 Electrophysiology

As mentioned above, we've inherited all Baseline parameters for I_{Ca_L} from the updated Bondarenko model[4]. To match the CaMKII-dependent increases in peak current ($\sim$ 20%), and fast inactivation time ($\sim$ 25%), we applied proportional shifts in G_{Ca_L} and $K_{pc,max}$. Initially, we altered the Baseline model to incorporate K^+ current representations from Li *et al.*[11], primarily for their parameterization to data collected at physiologic temperature. However, we found these representations to provide very strong overall repolarization, such that it was not possible to approach our recorded Baseline AP durations within reasonable ranges of the Ca^{2+}-handling parameters. As an alternative we retained the original Bondarenko formulations of all K^+ currents. We modeled CaMKII-specific effects at I_{to} as being solely due to I_{to_f}, primarily because the slow component appears only rarely murine cells[8]. Thus, the $\sim$ 35% reduction in total I_{to} observed by Wagner et al.,[20] was used to parameterize G_{to_f} in our Tg model, and in combination with changes to I_{Ca_L}, this was sufficient to recapitulate our APD_{50} data - Figure S3. G_{K1} was also reduced in line with the observations of Wagner *et al*. This combined with changes to calcium handling allowed a relative difference in APD_{90} that was similar to the experimental data. However, absolute APD_{90} was still shorter for both models than observed experimentally, and it is probable that the balance of currents during late repolarization in this model still favor repolarization slightly more strongly than is true for our isolated cells. Finally, the K_m for intracellular sodium binding of the N^+/K^+-ATPase ($K_{m,Nai}$) was reduced from 21 to 16.65 $mmol/L$ to maintain stable Na^+ handling in all three models[3].

2.2.3 β-adrenergic stimulation

Isoproterenol challenge was simulated with parameter changes representing established effects of β-adrenergic stimulation, and are presented in supplemental table 1. These parameter changes were applied to initial conditions taken from the final steady state of the Tg model, and the effects were allowed to develop over time as the model was paced through 50 beats. Briefly, the major changes were a 2-fold increase in G_{Ca_L}[18], 7 mV leftward shifts in I_{Ca_L} steady-state activation and inactivation, and a 20% increase in $G_{K_{ur}}$[10]. Also, as mentioned in section 3.6, because our experimental data suggest that transition to EADs is dependent upon SR Ca^{2+} release, we fixed all other parameters and progressively reduced K_{mr} and K_{mf} to slowly introduce PKA-dependent effects upon SR Ca^{2+} reuptake and whole-cell Ca^{2+} load. **Importantly, we did not implement any effects specifically of β-adrenergic regulation at I_{Na}. There are two well-established effects of this regulation on macroscopic I_{Na} (1) leftward shifts in steady activation and inactivation, (2) Increased peak I_{Na} conductance. Our reasoning for ignoring these effects were,**

respectively: (1) the leftward shifts in steady state activation and inactivation are equally likely to be secondary to activation of CaMKII during βAR stimulation, and subsequent CaMKII-dependent phosphorylation of $Na_V1.5$. Because these effects are already incorporated within the Grandi I_{Na} model we avoided additional leftward shifts due to PKA, (2) the increase in peak I_{Na} is thought to arise from trafficking of $Na_V1.5$ to the cell surface, and generally appear after $\sim$ 5 minutes[2]. Because our experiments generally were complete between 2-3 minutes after initiating βAR stimulation, we feel is it unlikely this mechanism could have contributed to the observed outcomes.

2.2.4 Model Implementation and Availability

All models were implemented in Matlab (Release 2013a), and solved with the adaptive implicit ODE solver ODE15s. Pacing current injection was simulated by 5 ms square pulses of 8.0 A/F amplitude, and was carried by K^+. All model code and data for this study are available at the CMRG website:
UCSD Cardiac Mechanics Research Group

References

[1] X. Ai, J. W. Curran, T. R. Shannon, D. M. Bers, and S. M. Pogwizd. Ca2+/calmodulin-dependent protein kinase modulates cardiac ryanodine receptor phosphorylation and sarcoplasmic reticulum Ca2+ leak in heart failure. *Circ. Res.*, 97(12):1314–1322, Dec. 2005.

[2] S. Baba, W. Dun, and P. A. Boyden. Can PKA activators rescue na+ channel function in epicardial border zone cells that survive in the infarcted canine heart? *Cardiovasc Res.*, 64(2):260–267, Nov. 2004.

[3] R. G. Berry, S. Despa, W. Fuller, D. M. Bers, and M. J. Shattock. Differential distribution and regulation of mouse cardiac Na+/K+-ATPase alpha1 and alpha2 subunits in T-tubule and surface sarcolemmal membranes. *Card. Res.*, 73(1):92–100, 2007.

[4] V. E. Bondarenko and R. L. Rasmusson. Transmural heterogeneity of repolarization and Ca2+ handling in a model of mouse ventricular tissue. *AJP-Heart And Circulatory Physiology.*, 299(2):H454–69, Aug. 2010.

[5] V. E. Bondarenko, G. P. Szigeti, G. C. L. Bett, S.-J. Kim, and R. L. Rasmusson. Computer model of action potential of mouse ventricular myocytes. *AJP-Heart And Circulatory Physiology.*, 287(3):H1378–403, Sept. 2004.

[6] J. Curran, M. J. Hinton, E. Ríos, D. M. Bers, and T. R. Shannon. Beta-adrenergic enhancement of sarcoplasmic reticulum calcium leak in cardiac myocytes is mediated by calcium/calmodulin-dependent protein kinase. *Circ. Res.*, 100(3):391–398, Feb. 2007.

[7] E. Grandi, J. L. Puglisi, S. Wagner, L. S. Maier, S. Severi, and D. M. Bers. Simulation of Ca-calmodulin-dependent protein kinase II on rabbit ventricular myocyte ion currents and action potentials. *Biophysical Journal.*, 93(11):3835–3847, Nov. 2007.

[8] W. Guo, H. Xu, B. London, and J. M. Nerbonne. Molecular basis of transient outward K+ current diversity in mouse ventricular myocytes. *J. Physiol.*, 521 Pt 3:587–599, Dec. 1999.

[9] M. Kohlhaas, T. Zhang, T. Seidler, D. Zibrova, N. Dybkova, A. Steen, S. Wagner, L. Chen, J. H. Brown, D. M. Bers, and L. S. Maier. Increased sarcoplasmic reticulum calcium leak but unaltered contractility by acute CaMKII overexpression in isolated rabbit cardiac myocytes. *Circ. Res.*, 98(2):235–244, Feb. 2006.

[10] G. R. G. Li, J. J. Feng, Z. Z. Wang, B. B. Fermini, and S. S. Nattel. Adrenergic modulation of ultrarapid delayed rectifier K+ current in human atrial myocytes. *Circ. Res.*, 78(5):903–915, May 1996.

[11] L. Li, S. A. Niederer, W. Idigo, Y. H. Zhang, P. Swietach, B. Casadei, and N. P. Smith. A mathematical model of the murine ventricular myocyte: a data-driven biophysically based approach applied to mice overexpressing the canine NCX isoform. *AJP-Heart And Circulatory Physiology*., 299(4):H1045–63, Sept. 2010.

[12] L. Livshitz, K. Acsai, G. Antoons, K. Sipido, and Y. Rudy. Data - Based Theoretical Identification of Subcellular Calcium Compartments and Estimation of Calcium Dynamics in Cardiac Myocytes. *J. Physiol*., June 2012.

[13] Y.-M. Lu, J. Huang, N. Shioda, K. Fukunaga, Y. Shirasaki, X.-M. Li, and F. Han. CaMKIIδB mediates aberrant NCX1 expression and the imbalance of NCX1/SERCA in transverse aortic constriction-induced failing heart. *PloS one*., 6(9):e24724, 2011.

[14] L. S. Maier, T. Zhang, L. Chen, J. DeSantiago, J. H. Brown, and D. M. Bers. Transgenic CaMKIIdeltaC overexpression uniquely alters cardiac myocyte Ca2+ handling: reduced SR Ca2+ load and activated SR Ca2+ release. *Circ. Res*., 92(8):904–911, May 2003.

[15] K. Maxwell, J. Scott, A. Omelchenko, A. Lukas, L. Lu, Y. Lu, M. Hnatowich, K. D. Philipson, and L. V. Hryshko. Functional role of ionic regulation of Na+/Ca2+ exchange assessed in transgenic mouse hearts. *Am. J. Physiol*., 277(6 Pt 2):H2212–21, Dec. 1999.

[16] G. F. Mitchell, A. Jeron, and G. Koren. Measurement of heart rate and Q-T interval in the conscious mouse. *Am. J. Physiol*., 274(3 Pt 2):H747–51, Mar. 1998.

[17] T. D. O'Connell, M. C. Rodrigo, and P. C. Simpson. Isolation and culture of adult mouse cardiac myocytes. *Methods molecular biology (Clifton, NJ)*., 357:271–296, 2007.

[18] T. R. Shannon, F. Wang, and D. M. Bers. Regulation of cardiac sarcoplasmic reticulum Ca release by luminal [Ca] and altered gating assessed with a mathematical model. *Biophysical Journal*., 89(6):4096–4110, Nov. 2005.

[19] T. R. Shannon, F. Wang, J. Puglisi, C. Weber, and D. M. Bers. A mathematical treatment of integrated Ca dynamics within the ventricular myocyte. *Biophysical Journal*., 87(5):3351–3371, Oct. 2004.

[20] S. Wagner, E. Hacker, E. Grandi, S. L. Weber, N. Dybkova, S. Sossalla, T. Sowa, L. Fabritz, P. Kirchhof, D. M. Bers, and L. S. Maier. Ca/calmodulin kinase II differentially modulates potassium currents. *Circulation: Arrhythmia Electrophysiology*., 2(3):285–294, May 2009.

[21] C. R. Weber, K. S. Ginsburg, K. D. Philipson, T. R. Shannon, and D. M. Bers. Allosteric regulation of Na/Ca exchange current by cytosolic Ca in intact cardiac myocytes. *J. Gen. Physiol*., 117(2):119–131, Feb. 2001.

[22] X. H. T. Wehrens, S. E. Lehnart, S. R. Reiken, and A. R. Marks. Ca2+/calmodulin-dependent protein kinase II phosphorylation regulates the cardiac ryanodine receptor. *Circ. Res.*, 94(6):e61–70, Apr. 2004.

3 Supplemental figures

Figure S1

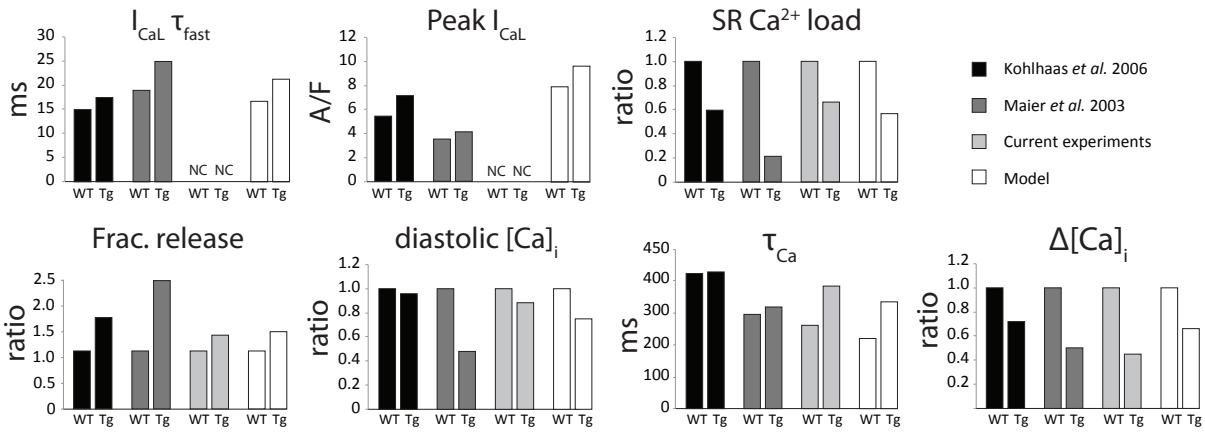

Figure S2

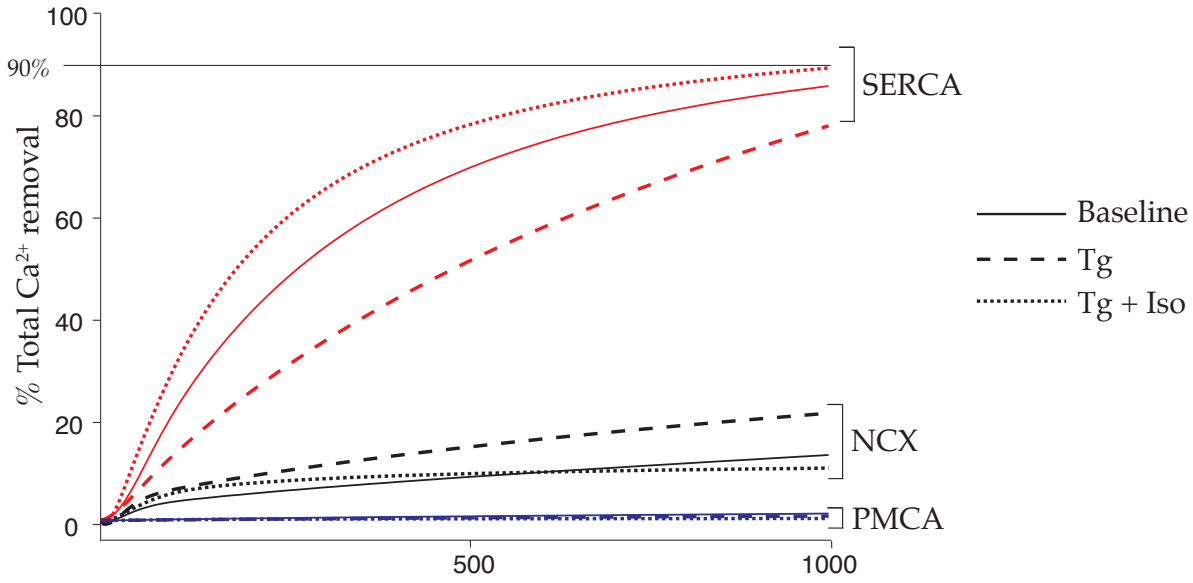
100
90%
80
60
40
20
0
% Total Ca2+ removal
500
1000
SERCA
NCX
PMCA
Baseline
Tg
Tg + Iso

Figure S3

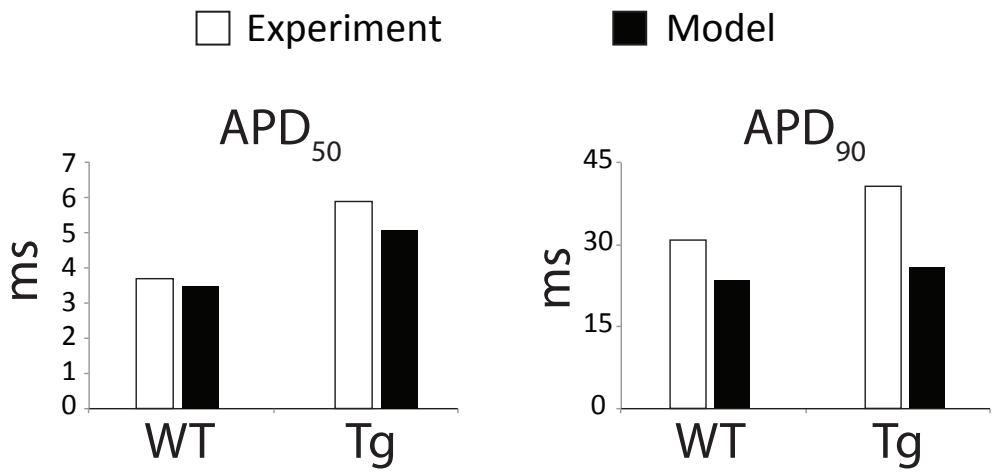
Experiment
Model
APD50
ms
7
6
5
4
3
2
1
0
WT
Tg
APD90
ms
45
30
15
0
WT
Tg

Figure S4

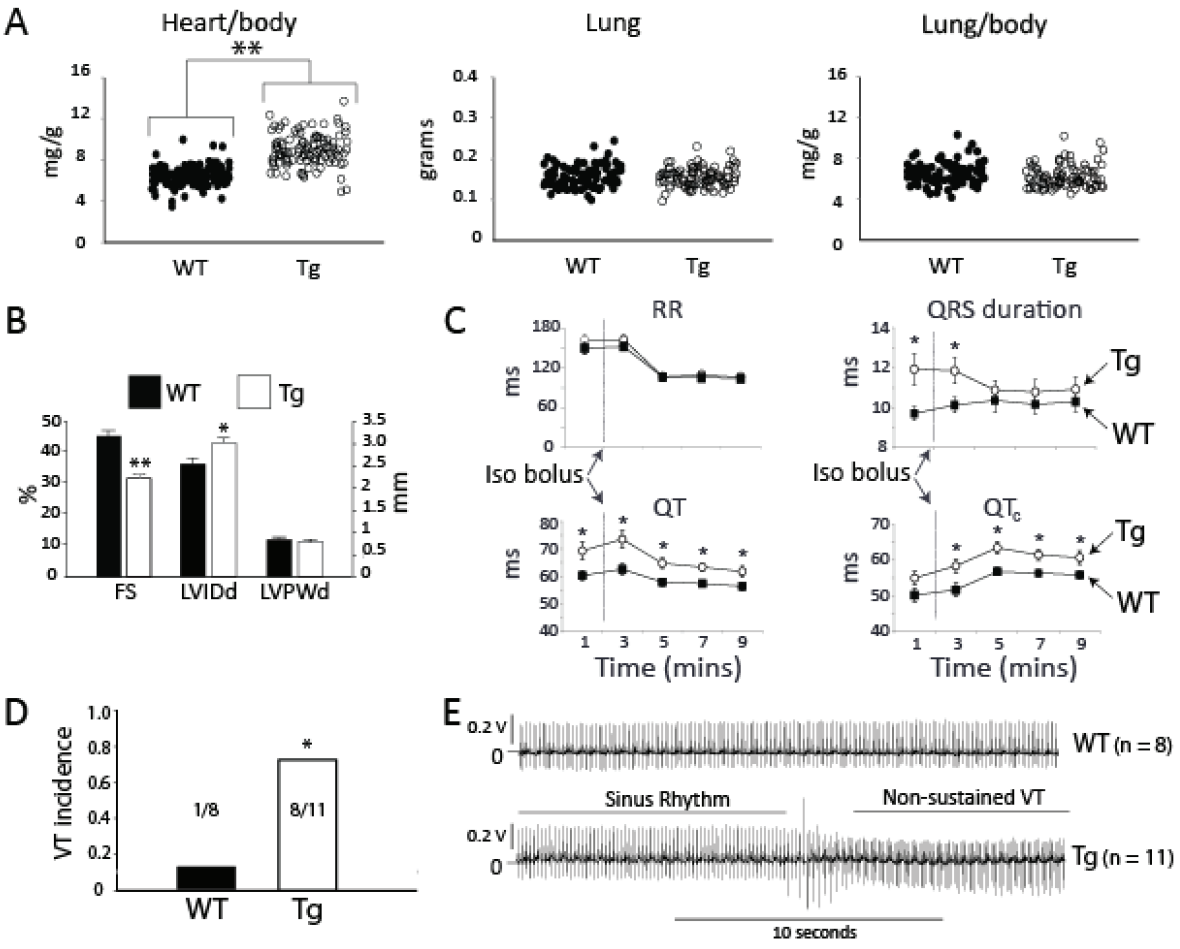
A
Heart/body
Lung
Lung/body
mg/g
grams
WT
Tg
B
WT
Tg
%
mm
FS
LVIDd
LVPWd
C
RR
QRS duration
ms
Iso bolus
QT
QTc
Time (mins)
D
VT incidence
1/8
8/11
E
0.2 v
WT (n = 8)
Sinus Rhythm
Non-sustained VT
Tg (n = 11)
10 seconds

Figure S5

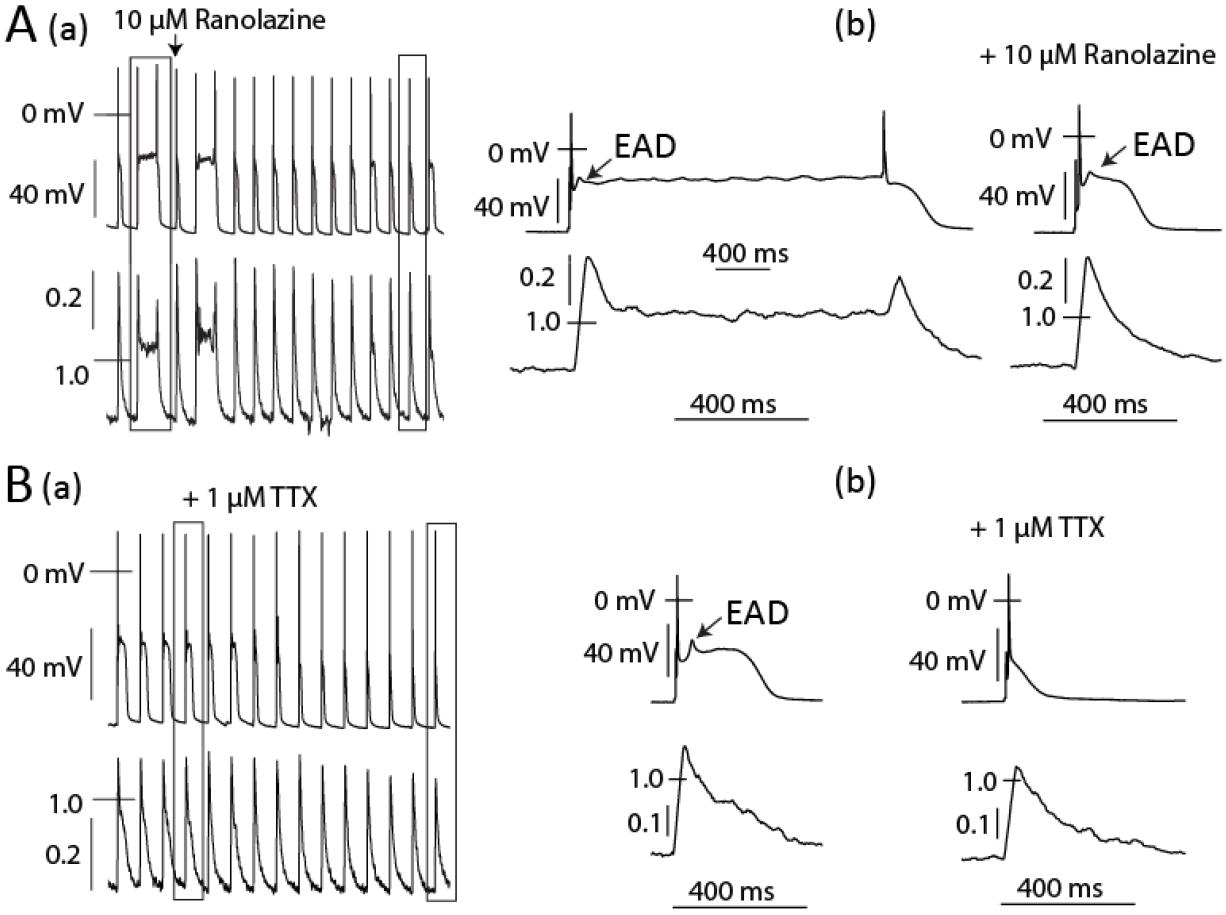
A (a)
10 μM Ranolazine
0 mV
40 mV
0.2
1.0
(b)
+ 10 μM Ranolazine
0 mV
EAD
40 mV
400 ms
0.2
1.0
400 ms
B (a)
+ 1 μM TTX
0 mV
40 mV
1.0
0.2
(b)
+ 1 μM TTX
0 mV
EAD
40 mV
1.0
0.1
400 ms

Figure S6

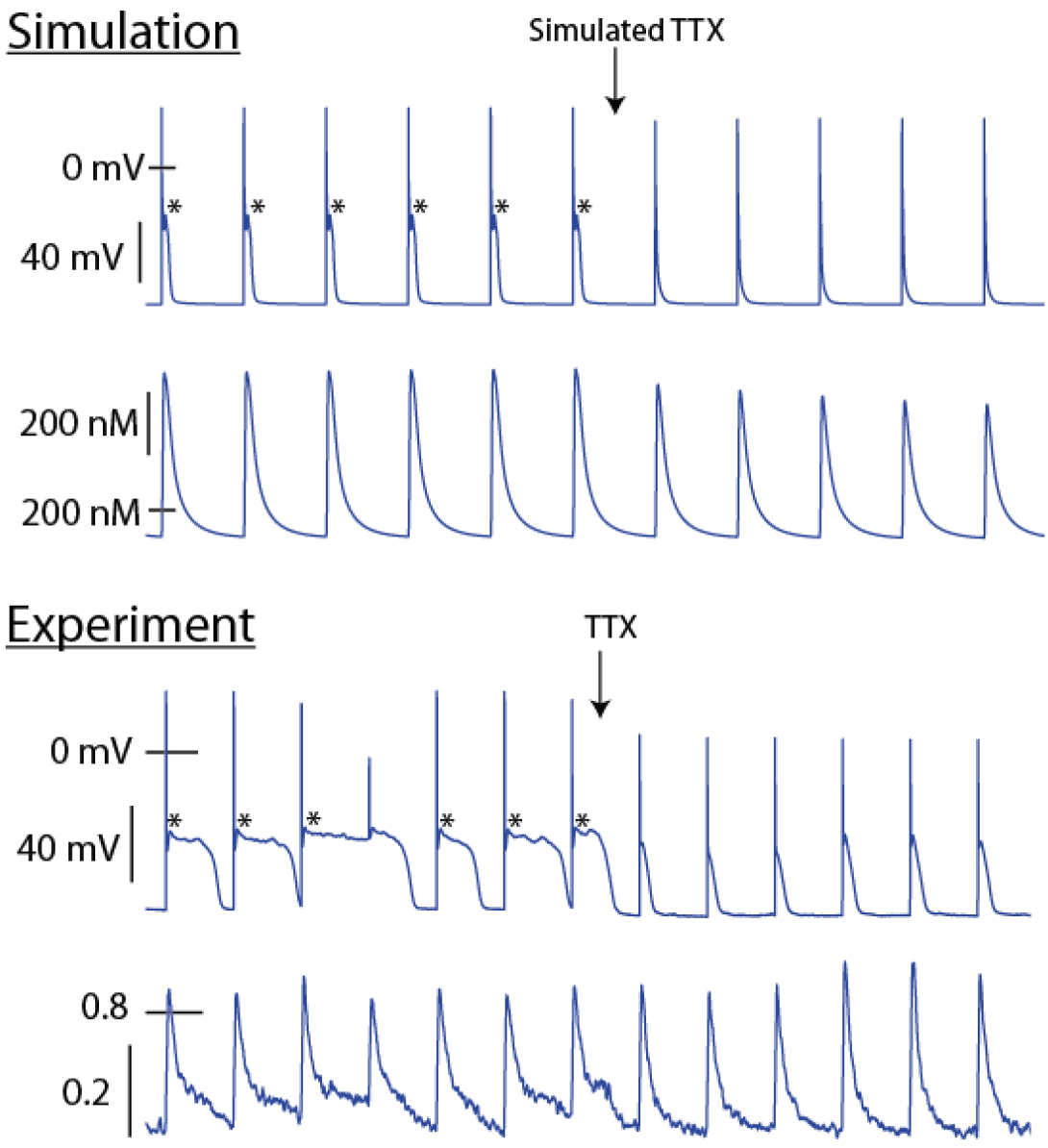
Simulation
Simulated TTX
0 mV
40 mV
200 nM
200 nM
Experiment
TTX
0 mV
40 mV
0.8
0.2

Figure S7

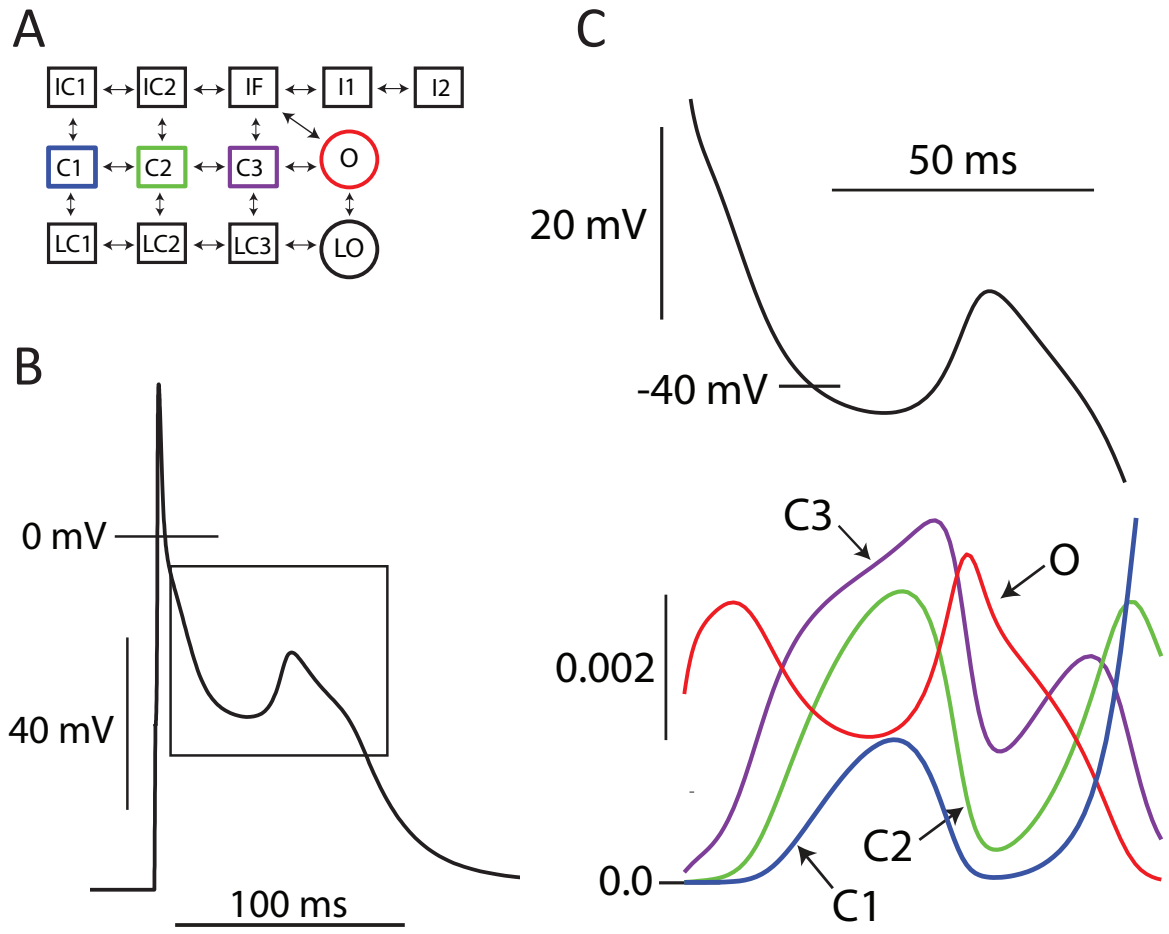
A
IC1
IC2
IF
I1
I2
C1
C2
C3
O
LC1
LC2
LC3
LO
B
0 mV
40 mV
100 ms
C
50 ms
20 mV
-40 mV
C3
O
0.002
0.0
C2
C1

Figure S8

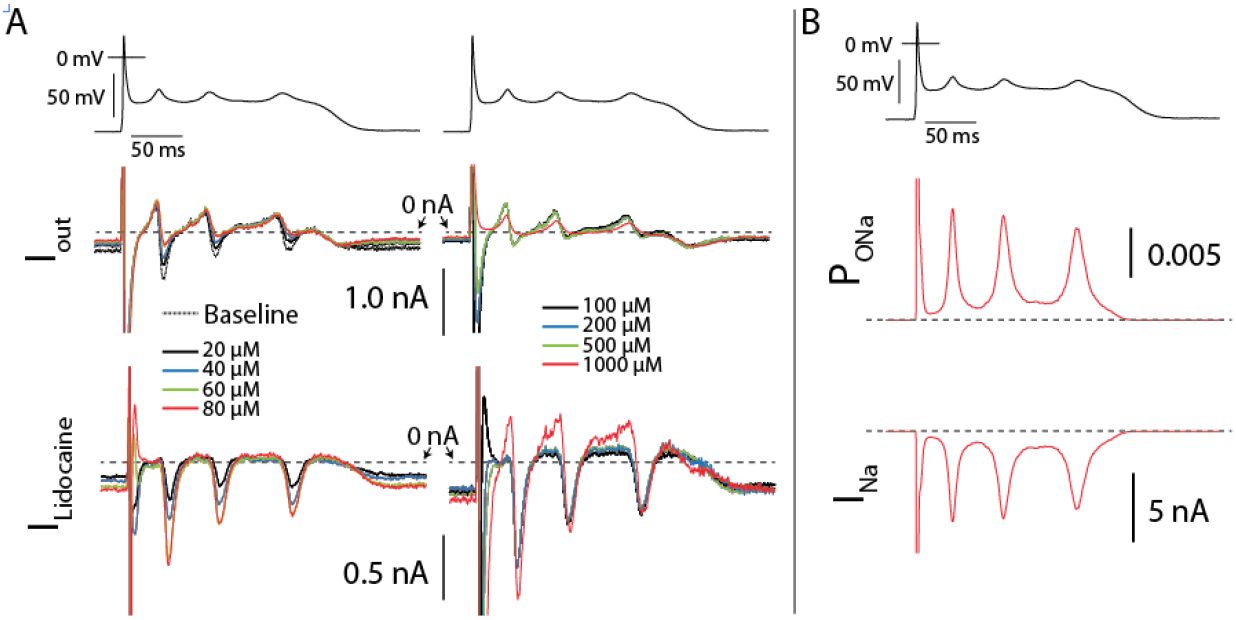
A
0 mV
50 mV
50 ms
0 nA
I out
1.0 nA
Baseline
20 µM
40 µM
60 µM
80 µM
100 µM
200 µM
500 µM
1000 µM
I Lidocaine
0 nA
0.5 nA
B
0 mV
50 mV
50 ms
P ONa
0.005
I Na
5 nA

Figure S9

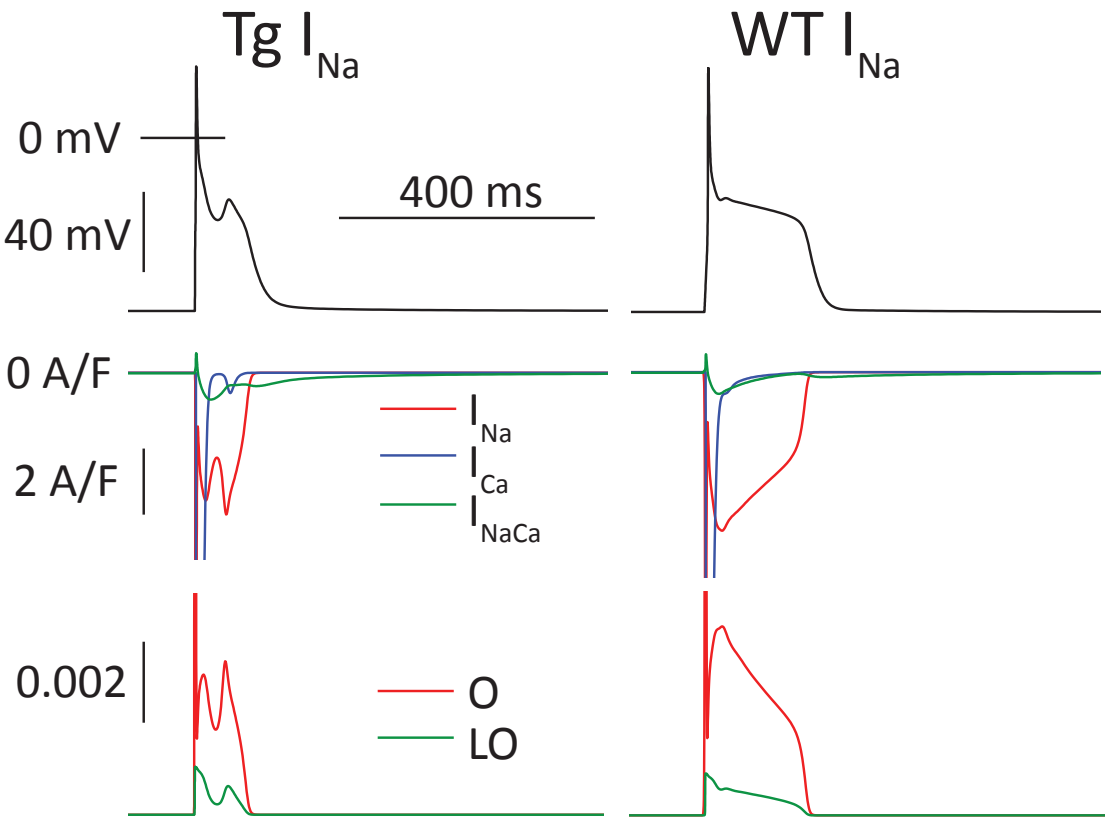

Figure S10

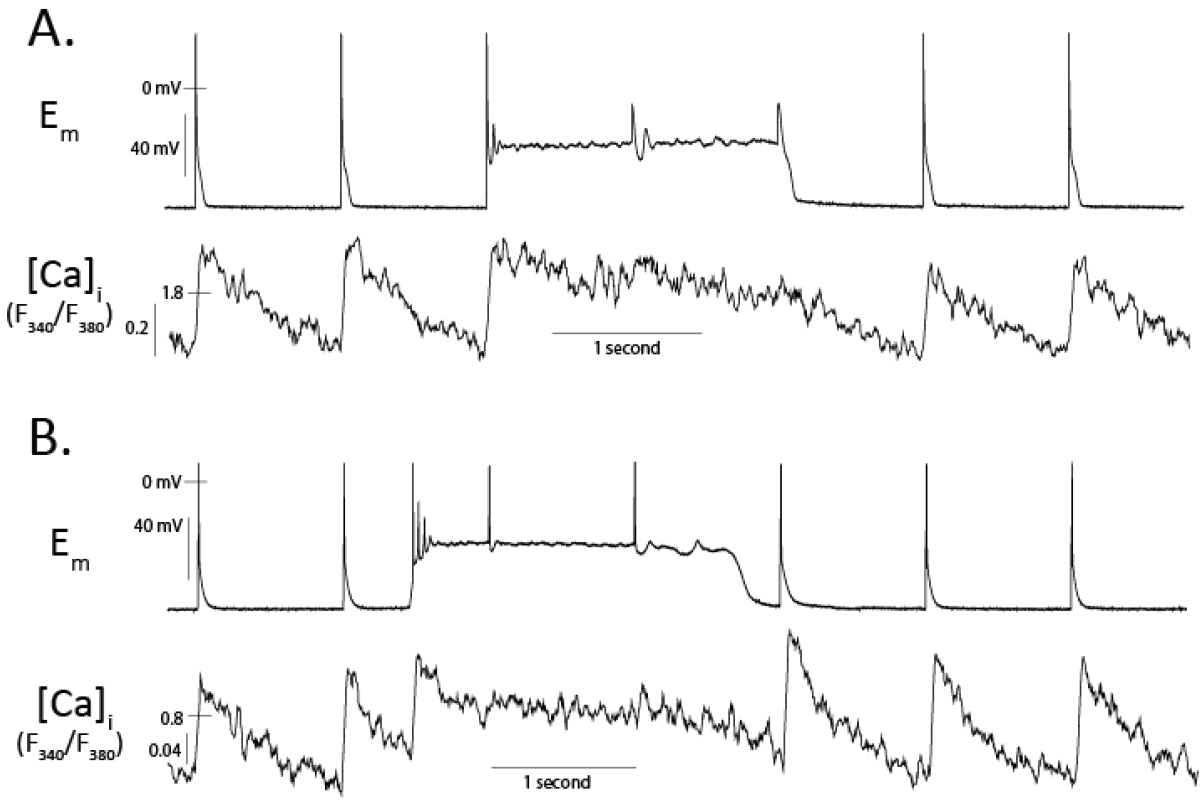
A.
0 mV
E_m
40 mV
$[Ca]_i$
(F_{340}/F_{380})
1.8
0.2
1 second
B.
0 mV
E_m
40 mV
$[Ca]_i$
(F_{340}/F_{380})
0.8
0.04
1 second

4 Supplemental figure legends

Table 1: Model Parameters. • Indicates parameters listed for the Baseline model that have been altered from the Bondarenko model. * indicates Tg specific effects. ** indicates Isoproterenol specific effects. *** indicates effects that are the combination of Tg- and Iso-specific effects. The parameters α_{left} and β_{left}, are part of the functions for α and β in the Bondarenko 2010 model[4]. These were (1) $\alpha = 0.4e^{(V+\alpha_{left})/15.0}$, and (2) $\beta = 0.13e^{-(V+\beta_{left})/18.0}$.

Figure S1: Comparison of steady-state model behavior with data from Kohlhaas *et al.*[9], Maier *et al.*[14], and herein. Tg data are normalized to Baseline for Fractional release(FR), SR Ca^{2+} load, diastolic Ca^{2+}, and $\Delta[Ca^{2+}]_i$, to allow comparison with fluorescence based measures of SR Ca^{2+} load[9,14], or our ratiometric Ca^{2+}-handling data. Absolute SR Ca^{2+} load for the Baseline model was 93 μmol/L cytosol. NC: data not collected herein.

Figure S2: Pathways of cytosolic Ca^{2+} removal at steady state in the Baseline, Tg, and Tg + Iso models. Time-courses are the cumulative integrals of net fluxes due to SERCA reuptake (red), and extrusion via NCX (black), or PMCA (blue).

Figure S3: Steady-state action potential duration in the Baseline and Tg models, and our experimental data.

Figure S4: Global cardiac phenotype: A. Kaplan-Meier curve showing onset of mortality in Tg mice. B. Heart:body mass (left) was increased in Tg mice, although both absolute lung mass (middle), and lung:body mass (right) were unchanged. C. Echocardiography indicates mild ventricular dilation and contractile dysfunction in pre-HF Tg mice; Tg (n = 10) vs. WT (n = 15) animals. D. Anesthetized electrocardiography at baseline and during intravenous isoproterenol (Iso, 25 μg/kg) challenge for Tg (n = 10) and WT (n = 14) animals. E. IP injection of epinephrine (2 mg/kg) and caffeine (120 mg/kg) elicited VT in Tg animals. F. Representative episode of non-sustained VT in a Tg animal. Heart rate increased from $\sim$390 beats/min at baseline to $\sim$430 beats/min shortly after epi/caff,

and then ∼600 beats/min during VT. All panels: ** $p < 0.001$, * $p < 0.05$. Group data are mean ± SEM.

Figure S5: Complete traces for the experimental cell in Figure 7 directly after application of 10 μM Ranolazine (A), and addition of 1 μM TTX to the bath (B). Right side of both panels shows the change in AP morphology resulting from the antagonist - selected APs are boxed at left. Ranolazine curtailed to the prolonged EAD phenotype but did not prevent the dynamics underlying EAD initiation. Conversely TTX at 1 μM or greater did eliminate EAD initiation.

Figure S6: A. Comparison of EAD prevention by TTX blockade in experiments and simulations. A. Imposing an acute 50% reduction of peak I_{Na} conductance (G_{Na} = 6.5 $mS.\mu F^{-1}$) to simulate rapid TTX application, abolishes EADs (indicated by asterisks *) in the Tg + Iso model. B. Similar rapid application of TTX abolishes EADs in an experimental cell.

Figure S7: Reactivation through canonical recovery from I_{Na} inactivation. A. The states of the Markovian I_{Na} model. B. Simulated action potential including an EAD as in Figure 6B(c). C. Magnified region of I_{Na} reactivation from B, including E_m (top) and state occupancies (bottom) for the canonical closed states (C1-C3), and the open state (O). Non-equilibrium reactivation is fueled by these canonical closed states.

Figure S8: The Tg I_{Na} model[20] exhibits reduced non-equilibrium reactivation during Iso-challenge compared to the WT I_{Na} model. Both simulations are performed in the transgenic cell model, but with either the WT (right) or Tg (left) I_{Na} representations. The WT I_{Na} model does not include the leftward shifts in steady-state activation and inactivation, enhanced late current, or sowed recovery from inactivation associated with CaMKII overexpression. The result is that the WT channel permits greater non-equilibrium reactivation, thus suggesting that the I_{Na}-dependent EADs we have observed do not rely specifically on CaMKII regulation of the channel.

Figure S9: A. Representative examples of sustained events. A. Triggered sustained events were generally non-terminating EADs, and therefore were treated as a special case of EAD. B. Representative example of the infrequent spontaneous sustained events.